Very Large-Scale Structures and Their Effects on the Wall Shear-Stress Fluctuations in a Turbulent Channel Flow up to $Re_\tau = 640$

Hiroyuki Abe[1]

Hiroshi Kawamura[†]

Department of Mechanical Engineering
Tokyo University of Science,
Noda-shi, Chiba 278-8510, Japan

Haecheon Choi

School of Mechanical and Aerospace
Engineering, Seoul National University,
Seoul 151-744, Korea

Direct numerical simulation of a fully developed turbulent channel flow has been carried out at three Reynolds numbers, 180, 395, and 640, based on the friction velocity and the channel half width, in order to investigate very large-scale structures and their effects on the wall shear-stress fluctuations. It is shown that very large-scale structures exist in the outer layer and that they certainly contribute to inner layer structures at high Reynolds number. Moreover, it is revealed that very large-scale structures exist even in the wall shear-stress fluctuations at high Reynolds number, which are essentially associated with the very large-scale structures in the outer layer. [DOI: 10.1115/1.1789528]

1 Introduction

The behavior of fluctuations of the wall flow variables in a turbulent boundary layer flow or in a turbulent channel flow is of fundamental interest in many applications involving drag, noise, and heat transfer. Among these, the wall pressure fluctuations have been intensively investigated by many researchers. The scaling law in the wall pressure power spectrum and the functional dependence of $p_{w_{rms}}/\tau_w$ on the Reynolds number have been fairly well established as discussed by Choi and Moin [1] and Farabee and Casarella [2], where p_w is the wall pressure fluctuations, τ_w is the mean shear stress at the wall, and the subscript rms denotes the root-mean-square value.

Unlike the wall pressure fluctuations, however, only limited information about the wall shear-stress fluctuations has been available, mainly because of measurement difficulties associated with the spatial resolution and frequency response of the probe and also with heat conduction to the wall. Therefore, in the experiment, a lot of difficulties have been encountered in determining the scaling law in the wall shear-stress (τ_1 and τ_3) power spectra and the functional dependence of $\tau_{1_{rms}}/\tau_w$ or $\tau_{3_{rms}}/\tau_w$ on the Reynolds number (see Jeon et al. [3]), where $\tau_1 = \mu \partial u'/\partial y|_w$ and $\tau_3 = \mu \partial w'/\partial y|_w$ are the two components of the wall shear-stress fluctuations, u' and w' are the streamwise and spanwise velocity fluctuations, respectively, y is the distance from the wall, and μ the dynamic viscosity. Moreover, the studies focusing on the wall flow variables from direct numerical simulation (DNS) have been limited mostly to $Re_\tau = u_\tau \delta/\nu = 180$ [1,3,4], where u_τ is the friction velocity, δ the channel half width, and ν the kinematic viscosity.

The importance of the contribution from the outer layer to the inner layer has been indicated by several experimental studies in wall-bounded turbulence at high Reynolds numbers [5–10]. These studies revealed that large-scale or very large-scale motions in the outer layer affect the near-wall region and that this effect increases with increasing Reynolds number. For example, Bullock et al. [5]

performed an experiment in a turbulent pipe flow at $Re_\tau = 2600$ and found from the premultiplied frequency spectra of streamwise velocity fluctuations that large scale (low frequency) turbulence fluctuations extend over the majority of the radial region. Naguib and Wark [6] also found that the contribution of the outerlayer-structures to the streamwise velocity fluctuations increases with increasing Reynolds number. Hites [7] conducted an experiment in a turbulent boundary layer at $Re_\tau \approx 1500-6000$ and indicated that the premultiplied frequency spectra of streamwise velocity fluctuations show a bimodal distribution in the range of $38 < y^+ < 100$. Kim and Adrian [8] measured the streamwise velocity in a turbulent pipe flow at $Re_\tau = 1058$, 1984, and 3175 and obtained the premultiplied wave number spectrum of the streamwise velocity fluctuations derived from the frequency spectrum using Taylor's hypothesis. They showed that the premultiplied wave number spectra have a bimodal distribution and the characteristic wavelength of the large-scale mode increases through the logarithmic layer. Moreover, they found that very large-scale motions corresponding to approximately 12–14 times the pipe radius exist in that region. Osterlund [9] observed the effect from the outer layer even in the wall flow variables such as the wall shear stress by investigating the two-point correlation. Metzger and Klewicki [10] investigated the near-wall turbulence quantities such as the streamwise velocity and its gradient for a turbulent boundary layer. They found that the influence of the low frequency components, i.e., large-scale structures, on the turbulence statistics increases with increasing Reynolds number.

Owing to the recent rapid increase in computer power, DNSs of turbulent channel flow have been performed for relatively high Reynolds numbers (see, for example, Antonia and Kim [11], Moser et al. [12], and Abe et al. [13]), where the Reynolds-number effect on the root-mean-square velocity and vorticity fluctuations inside the channel was carefully studied. However, since these studies were performed with relatively small computational boxes, the effects of very large-scale structures in the outer layer on turbulence quantities were not clearly examined.

More recently, with the aid of huge computer memory, DNSs with large computational boxes have been carried out by del Álamo and Jiménez [14,15] and Abe and Kawamura [16]. del Álamo and Jiménez [14,15] indicated that very large-scale structures of streamwise velocity fluctuations span most of the channel height and penetrate into the buffer region. Also, Jiménez et al. [17] showed that, when the flow in the outer layer is artificially

---

Table 1 Computational box size, grid points, spatial resolution, and sampling time period

Re_τ	180	395	640
$L_x \times L_y \times L_z$	$12.8\delta \times 2\delta \times 6.4\delta$	$12.8\delta \times 2\delta \times 6.4\delta$	$12.8\delta \times 2\delta \times 6.4\delta$
$L_x^+ \times L_y^+ \times L_z^+$	$2304 \times 360 \times 1152$	$5056 \times 790 \times 2528$	$8192 \times 1280 \times 4096$
$N_x \times N_y \times N_z$	$256 \times 128 \times 256$	$512 \times 192 \times 512$	$1024 \times 256 \times 1024$
$\Delta x^+, \Delta y^+, \Delta z^+$	$9.00, 0.20 \sim 5.90, 4.50$	$9.88, 0.15 \sim 6.52, 4.94$	$8.00, 0.15 \sim 8.02, 4.00$
Tu_m/L_x	49	50	14

removed, the near-wall turbulence structures become infinitely long, but the averaged turbulence quantities do not noticeably change in the near-wall region.

In the present study, we have performed DNS of turbulent channel flow at three Reynolds numbers, $Re_\tau = 180$, 395, and 640, with a large computational box ($L_x \times L_z = 12.8\delta \times 6.4\delta$) in order to include very large-scale structures existing in the outer layer. The computational box size of our previous study [13] for $Re_\tau = 640$ was $L_x \times L_z = 6.4\delta \times 2\delta$ [$4096 \times 1280(\nu/u_\tau)^2$], which contained sufficient numbers of near-wall (more than ten) streaky structures in the spanwise direction, but was not large enough to include sufficient numbers of very large-scale structures in the outer layer. Accordingly, the difference between the results from the present and previous computations should be attributed to the effects of the very large-scale structures existing in the outer layer. Hence, the purpose of the present paper is to investigate the very large-scale structures and their effects on the turbulence quantities, especially on the wall shear-stress fluctuations, from root-mean-square values, power spectra and instantaneous flow fields.

2 Numerical Procedure

The flow in the present study is a fully developed turbulent channel flow driven by a streamwise mean pressure gradient. In the present computation, a fractional step method proposed by Dukowics and Dvinsky [18] is adopted, and a semi-implicit time advancement is taken (the Crank–Nicolson method for the viscous terms with wall-normal derivatives and the second-order Adams–Bashforth method for the other terms). For the spatial discretization, a fourth-order central difference scheme proposed by Morinishi et al. [19] is adopted in the streamwise and spanwise directions, and the second-order central difference scheme is used in the wall-normal direction. Further details of the present numerical method can be found in Abe et al. [13].

As pointed out by Jiménez [20], very large-scale structures existing near the center of the channel have a spanwise size of 2δ. Recently, del Álamo and Jiménez [14,15] reported that very large-scale structures of $2-5\delta$ in length in the streamwise direction exist in the outer layer at a relatively high Reynolds number of $Re_\tau = 550$. They also indicated that at least ten washout times are needed to obtain stationary statistics related to large scales. Therefore, irrespective of the Reynolds number, the size of the present computational box ($L_x \times L_y \times L_z$) was chosen to be $12.8\delta \times 2\delta \times 6.4\delta$ in the streamwise (x), wall-normal (y), and spanwise (z) directions, respectively, in order to include quite a few very large-scale structures in our computational box. The integration time for statistical sampling was set to be more than ten washout times for all the cases. The computational box size, number of grid points (N_x, N_y, N_z), spatial resolution ($\Delta x, \Delta y, \Delta z$) and sampling time period (Tu_m/L_x) are given in Table 1, where u_m denotes the bulk mean velocity. Accuracy at the present spatial resolution has already been confirmed by Kawamura et al. [21], Abe et al. [13], and Abe and Kawamura [16].

3 Results and Discussion

3.1 Very Large-Scale Structures

3.1.1 Effects of Very Large-Scale Structures on Mean Flow Variables and Turbulence Quantities. Before we discuss the behavior of very large-scale structures in the outer layer, we examine their effects on the mean flow variables and the root-mean-square velocity fluctuations for $Re_\tau = 640$ by comparing the present results with those from our previous study [13], in which a smaller computational box was used for the same Reynolds number. In wall-bounded turbulence, one of the most important quantities is the friction coefficient. It is defined as

$$C_f = \frac{\tau_w}{\frac{1}{2}\rho u_m^2}. \tag{1}$$

The friction coefficient in the present study for $Re_\tau = 640$ is $C_f = 5.47 \times 10^{-3}$, whereas the one in the previous study [13] for $Re_\tau = 640$ was $C_f = 5.42 \times 10^{-3}$. The difference is less than 1%.

The mean velocity distribution has also been investigated and is shown in Fig. 1. The experimental result of Hussain and Reynolds [22] and the DNS results of Moser et al. [12] in a turbulent channel flow at $Re_\tau = 590$ and of Spalart [23] in a turbulent boundary layer at $Re_\tau \approx 650$ are also included for comparison. Note that a superscript + denotes a variable normalized by wall units. It can be seen from Fig. 1 that agreement between the present and previous results is excellent. Other mean quantities were also compared, but their differences were also very small.

The root-mean-square values of the streamwise, wall-normal and spanwise velocity fluctuations, u'_{rms}, v'_{rms}, and w'_{rms}, for $Re_\tau = 640$ are compared with those of the previous studies [12,13,15,22] and are shown in Fig. 2. Again, agreement with the data at the same Reynolds number [13,22] is excellent except for
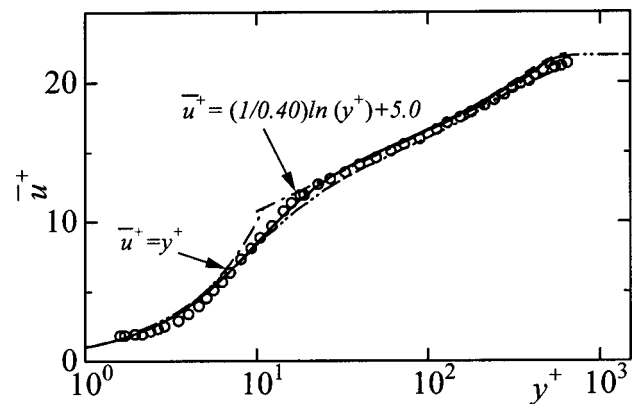
Fig. 1 Mean velocity distribution for $Re_\tau = 640$. (——), present; (— — —), Abe et al. [13]; (- - -); Moser et al. [12] for $Re_\tau = 590$; (–··–), Spalart [23] for $Re_\tau \approx 650$; (○) Hussain and Reynolds [22] for $Re_\tau = 640$.
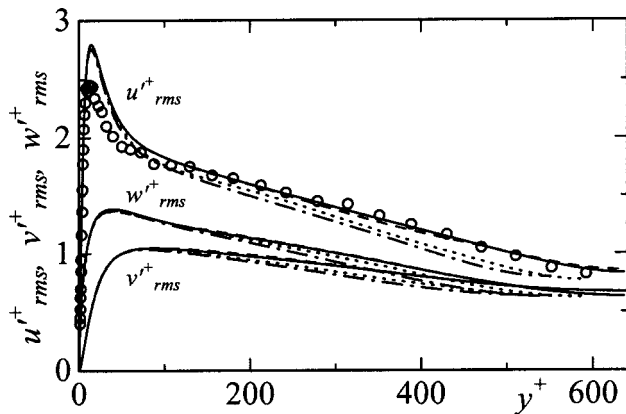
Fig. 2 Root-mean-square velocity fluctuations for $Re_\tau=640$. (——), present; (— — —), Abe et al. [13]; (- - -), Moser et al. [12] for $Re_\tau=590$; (—·—), del Álamo and Jiménez [15] for $Re_\tau=550$; (◯), Hussain and Reynolds [22] for $Re_\tau=640$.

Fig. 4 One-dimensional spanwise wave number power spectra of u' and w' for $Re_\tau=640$ at $y^+=5.38$ normalized by u_τ and δ in linear scales. (——), present; (— — —), Abe et al. [13]; (- - -), Moser et al. [12] for $Re_\tau=590$ $y^+=5.34$.

the near-wall streamwise velocity fluctuations, where the measurement with a hot wire is very difficult. Moreover, the present result agrees well with those of the other previous DNS studies at slightly different Reynolds numbers [12,15] in the near-wall region, although a small difference is found in the outer layer because of the difference in Re_τ.

Thus, one can conclude that the effect of the computational box size, in other words, very large-scale structures, is negligibly small for the mean flow variables and the second-order turbulence statistics within the limit of the Reynolds numbers investigated here.

We further investigate the effect of very large-scale structures on energy spectra in the inner and outer layers. The energy spectra of u', v', and w' are defined as

$$\int_0^\infty \phi(k_x)dk_x = \int_0^\infty \phi(k_z)dk_z = u'^2_{\text{rms}}, v'^2_{\text{rms}} \text{ or } w'^2_{\text{rms}}, \qquad (2)$$

where $\phi(k_x)$ and $\phi(k_z)$ are the energy spectra, and k_x and k_z are the wave numbers in the x and z directions, respectively. Figure 3 shows the energy spectra of the velocity fluctuations for $Re_\tau=640$ at $y^+\approx5$ together with those from the previous studies [12,13]. Excellent agreement with the previous results is observed at intermediate and high wave numbers, whereas a small but no-

ticeable difference is found at low wave numbers, especially for the spanwise energy spectra of u' and w'. The low-wave number behavior of the spanwise energy spectra of u' and w' is shown in Fig. 4, which is scaled with u_τ and δ and is drawn in linear scales. In Fig. 4, a large local peak is clearly observed in the spanwise spectra at a low wave number from the present data, whereas a less prominent peak is observed in the previous studies [12,13]. This difference is closely associated with very large-scale structures in the outer layer. Also, we see a number of small local peaks at low wave numbers, which could be due to statistical noise, as will be discussed later. The present comparison suggests that the computational box size used in this study should be required to capture the effect of the outer layer structures on the near-wall flow behavior. Nevertheless, when the energy spectra are integrated for the whole range of wave numbers, the differences in the mean-square values are ~3%. In summary, within the Reynolds number range investigated, the very large-scale structures in the outer layer have little effect on the time-averaged near-wall turbulence quantities, but they clearly exist even in the near-wall region and contribute to the energy at low wave numbers.

An examination of very large-scale structures in the outer layer using DNS requires a large computational box. In this region, the longest and widest structures are expected for the streamwise and spanwise velocities, respectively. This is because streamwise and spanwise directions are not constrained in the present configuration. Although the present computational box was chosen to be as large as possible, the box size at $Re_\tau=640$ ($L_x \times L_z = 12.8\delta \times 6.4\delta$) is half in the streamwise and spanwise directions of that of del Álamo and Jiménez [14,15] at $Re_\tau=550$ ($L_x \times L_z = 8\pi\delta \times 4\pi\delta$). Therefore, the validity of the present computational box size for $Re_\tau=640$ must be investigated. Figure 5 shows the streamwise premultiplied spectrum of u' and spanwise premultiplied spectrum of w' in the outer layer for $Re_\tau=640$, together with those of del Álamo and Jiménez [14] for $Re_\tau=550$. Here, the premultiplied spectra are defined as

$$\int_0^\infty k_x\phi(k_x)d(\log \lambda_x) = \int_0^\infty k_z\phi(k_z)d(\log \lambda_z) = u'^2_{\text{rms}} \text{ or } w'^2_{\text{rms}}, \qquad (3)$$

where $\lambda_x(=2\pi/k_x)$ and $\lambda_z(=2\pi/k_z)$ are the streamwise and spanwise wavelengths, respectively. In spite of the slight differences in the wall-normal locations where the spectra are obtained and the Reynolds numbers adopted, agreement between the present study and that of del Álamo and Jiménez [14] is very good, i.e., the peak values of the premultiplied spectra and the
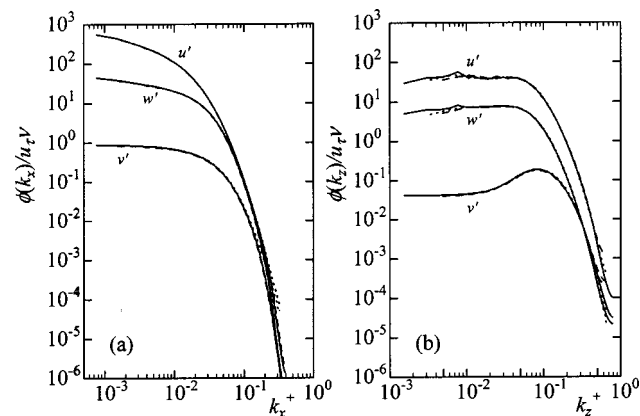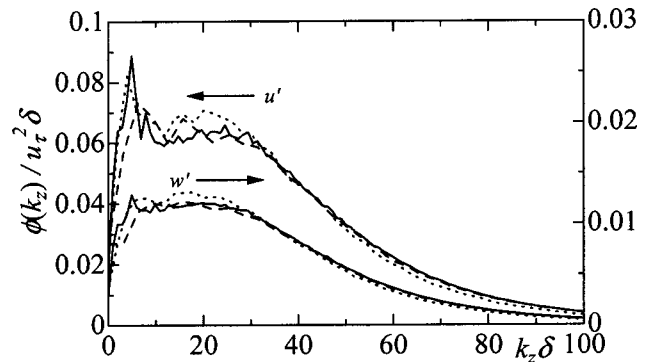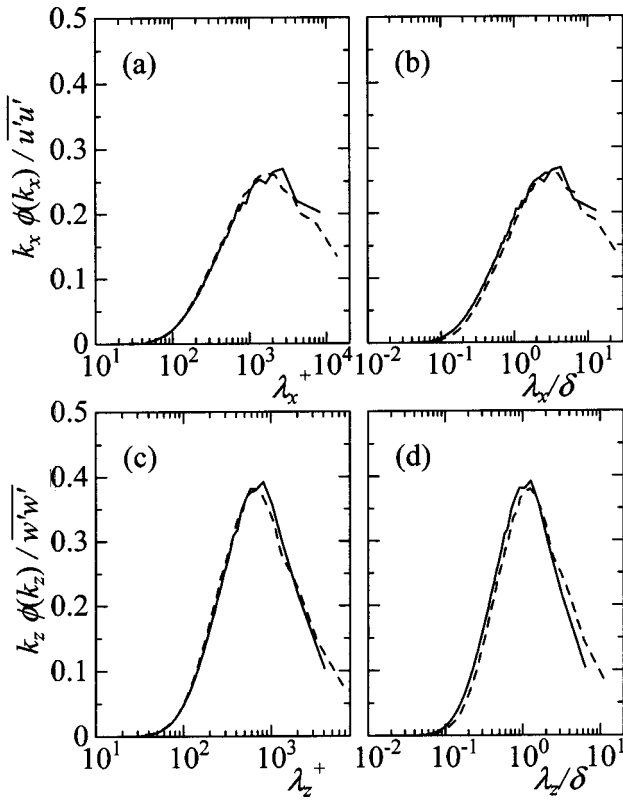

Fig. 3 One-dimensional wave number energy spectra of velocity fluctuations for $Re_\tau=640$ at $y^+=5.38$ in wall units: (a) streamwise wave number; (b) spanwise wave number. (——), present; (— — —), Abe et al. [13]; (- - -), Moser et al. [12] for $Re_\tau=590$ at $y^+=5.34$.

Fig. 5 Streamwise and spanwise premultiplied spectra of u' and w', $k_x\phi(k_x)/\overline{u'u'}$ and $k_z\phi(k_z)/\overline{w'w'}$, in the outer layer: (a), (b) $k_x\phi(k_x)/\overline{u'u'}$; (c), (d) $k_z\phi(k_z)/\overline{w'w'}$. (———), present for Re_τ=640 at y/δ=0.47 (y^+=298.2); (— — —), del Alamo and Jiménez [14] for Re_τ=550 at y/δ=0.5 (y^+=275).

energy at short wavelengths agree well with those of del Álamo and Jiménez [14]. Moreover, no artificial energy contamination is observed at long wavelengths.

Considering that the area under the premultiplied spectrum represents the mean-square velocity fluctuations as shown by Eq. (3), the present streamwise box size is not still enough to contain all the large-scale contributions [Figs. 5(a) and 5(b)], whereas the present spanwise box size seems to be quite sufficient [Figs. 5(c) and 5(d)]. It can be roughly estimated from Figs. 5(a) and 5(b) that one needs at least 100δ as a proper streamwise box size in order to obtain zero energy at the longest streamwise wavelength, at which point the simulation becomes very expensive.

3.1.2 Spanwise Very Large Scales. The large-scale structures are often referred to as the large-scale motions (LSMs) existing in the outer layer of the flow (see, for example, Falco [24]; Brown and Thomas [25]), and many experimental studies on the LSMs have been conducted for turbulent pipe, boundary layer and channel flows (see, for example, Kim and Adrian [8]; Adrian et al. [26]; Liu et al. [27]). Moreover, Kim and Adrian [8] found that very large-scale motions (VLSMs), which are much longer than the LSMs exist in the outer layer in a turbulent pipe flow. These studies mainly focused on the behavior of the LSMs or the VLSMs in the streamwise direction. On the other hand, some experimental studies have been performed on the spanwise organization of near-wall turbulence (see, for example, Smith and Metzler [28]), but little information is available for the spanwise behavior of large- or very large-scale structures in the outer layer from experiments (see, for example, Nakagawa and Nezu [29]). Therefore, we investigate here the behavior of the VLSMs in the spanwise direction with the aid of DNS.
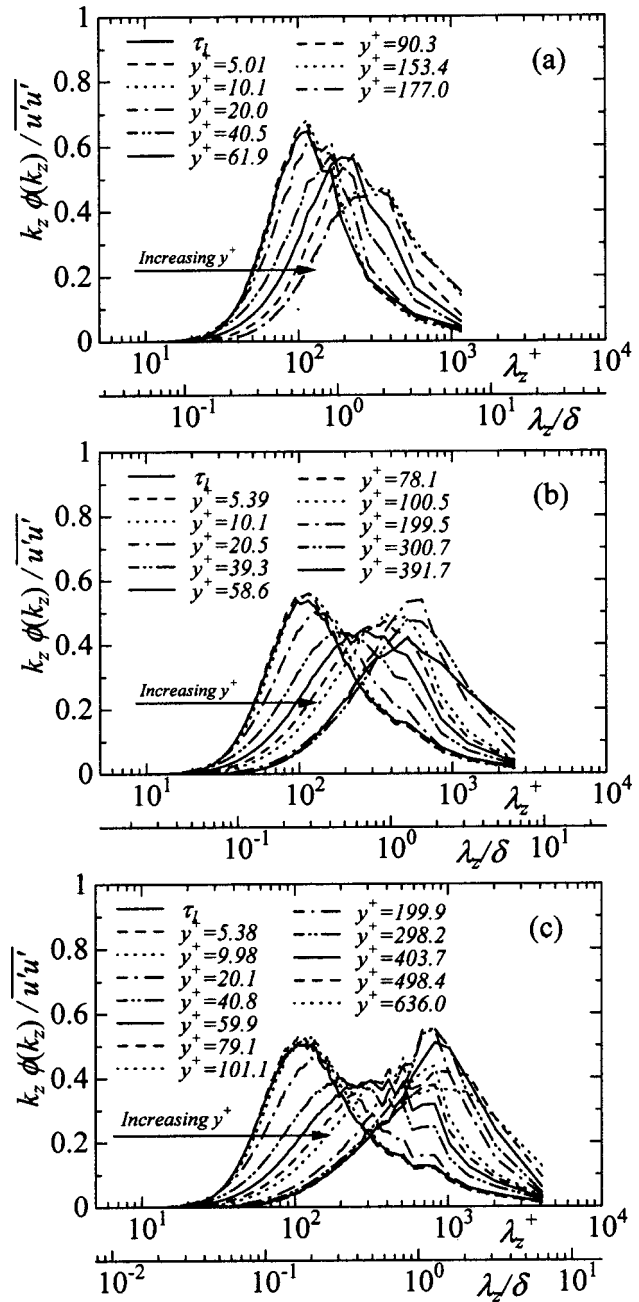
Fig. 6 Spanwise premultiplied energy spectra of the streamwise velocity fluctuations $k_z\phi(k_z)/\overline{u'u'}$: (a) Re_τ=180; (b) Re_τ=395; (c) Re_τ=640

Figure 6 shows the spanwise pre-multiplied energy spectra of the streamwise velocity fluctuations for Re_τ=180, 395, and 640. The spanwise premultiplied spectra of τ_1 are also included in this figure. Note that the peak location in the premultiplied spectrum corresponds to the wavelength of the energy-containing eddy (Perry et al. [30]). In the near-wall region (up to y^+=10), the premultiplied spectra of u' are nearly identical to that of τ_1 for each Reynolds number and their peaks are found at $\lambda_z^+ \approx 100$. Moving away from the wall, the peak position in the spectra of u' shifts to a longer wavelength. With increasing Reynolds number, the small and large scales corresponding to the energy-containing eddies in the near-wall and outer layer regions, respectively, are more clearly separated, and broad peaks appear between these two regions (e.g., at y^+=60–100 for Re_τ=640). Jiménez [20] pointed out that a very large-scale structure with a spanwise wavelength of
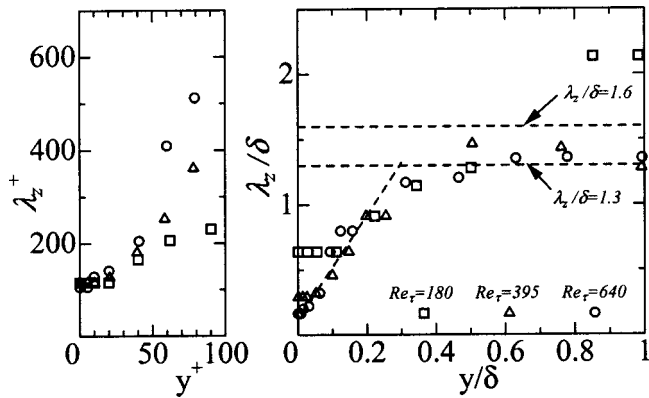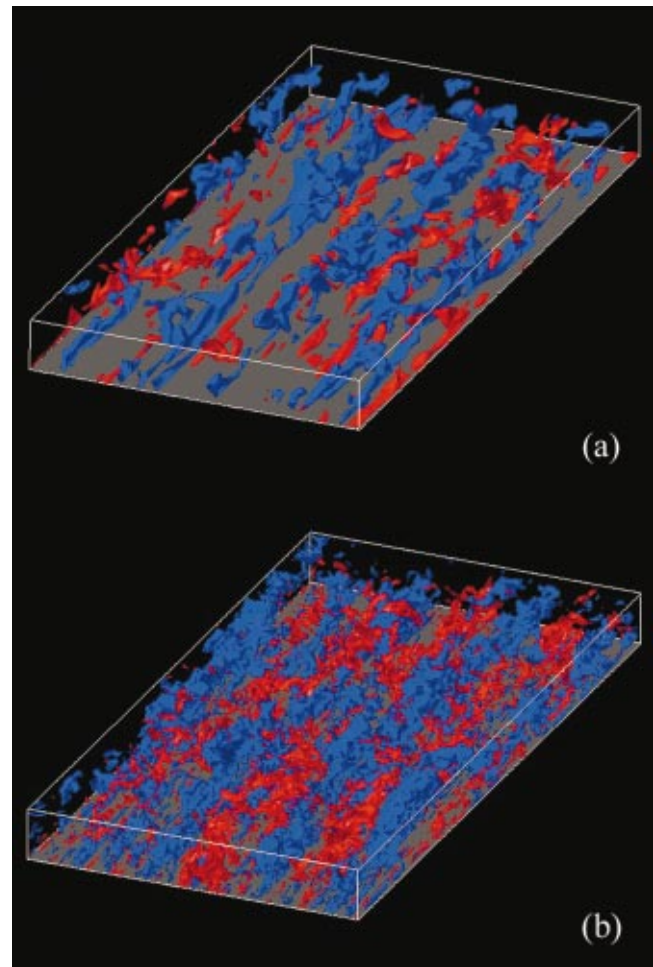
Fig. 7 Spanwise wavelengths of the most energetic eddies obtained from the premultiplied energy spectra of u' for Re_τ =180, 395, and 640

Fig. 8 Iso-surfaces of the instantaneous streamwise velocity fluctuations normalized by their own rms value at each y^+ for Re_τ=180 and 640: (a) Re_τ=180; (b) Re_τ=640 (red), u'/u'_{rms} >1.75; (blue), u'/u'_{rms}<−1.75. The boxes visualized here are $12.8\delta \times \delta \times 6.4\delta$ in the streamwise, wall-normal and spanwise directions, corresponding to those of $2304 \times 180 \times 1152(\nu/u_\tau)^3$ and $8192 \times 640 \times 4096(\nu/u_\tau)^3$ for Re_τ=180 and 640, respectively.

around 2δ exists at the midheight to the channel center. The present result indicates the same trend with a more definite determination of its wavelength as 1.3–1.6δ (see the peak location for $y/\delta=0.5$). It is interesting to notice that the near-wall premultiplied spectra show a local peak at the wavelength corresponding to the very large-scale structures for Re_τ=640 but not for Re_τ =180, indicating that the VLSMs in the outer layer contribute more to the inner layer structures with increasing Reynolds number.

The spanwise wavelengths of the most energetic eddies (MEW), for all three Reynolds numbers (Re_τ=180, 395, and 640) are obtained from Fig. 6 and are presented in Fig. 7. Note that when the premultiplied spanwise spectrum shows a clear peak we have taken the most energetic wavelength, while when the spectrum shows a broad peak we have computed a least-square interpolating polynomial in the region where the spectrum shows the most energetic power. The behavior of the wavelength of the most energetic eddy can be divided into three regions from Fig. 7. In the central region ($0.3 < y/\delta < 1$), the MEW stays essentially at a constant value of 1.3–1.6δ. From $y^+=20$ to $y/\delta \approx 0.3$, the MEW is linearly proportional to the wall-normal distance from the wall, agreeing well with the experimental result of Nakagawa and Nezu [29] and the DNS result of del Álamo and Jiménez [15]. This lower bound ($y^+=20$) seems to be scaled well with wall units, while the upper bound ($y/\delta \approx 0.3$) may be scaled with the outer variable δ. Finally, in the wall vicinity ($y^+ < 20$), the MEW remains constant at $\lambda_z^+ \approx 100$ that is the well-known spanwise separation distance of the near-wall streaky structures [28].

3.1.3 Visualization of Very Large-Scale Structures. To visualize the VLSMs in the outer layer, iso-surfaces of the instantaneous streamwise velocity fluctuations normalized by their own rms value at each y^+ for Re_τ=180 and 640 are shown in Fig. 8. This normalization is done because when the streamwise velocity fluctuations are normalized by the friction velocity, the structures emerge only in the wall vicinity due to the strong intensity there, and thus no structure can be captured in the outer region. It is seen from Fig. 8 that the VLSMs appear in the outer layer for both Reynolds numbers and as expected the high Reynolds number case shows a wider range of scales. The high- and low-speed regions appear with a spanwise spacing of about 1.3–1.6δ and with a streamwise extent larger than 3δ. This streamwise structure corresponds to those obtained from the measurements in pipe and channel flows (Kim and Adrian [8]; Liu et al. [27]) and from the DNS of a channel flow (del Álamo and Jiménez [14,15]).

4 Wall Shear-Stress Fluctuations

4.1 Root-Mean-Square Values. The rms values of the wall shear-stress fluctuations (τ_1 and τ_3) normalized by τ_w for Re_τ =180, 395, and 640 are given in Fig. 9, together with those obtained from DNS [3,11,31–34] and experiment [35] for the channel flow. The present result agrees very well with those of other DNS and experiment. The increase in $\tau_{1_{rms}}$ from Re_τ=180–640 is smaller ($\sim$11%) than that of $\tau_{3_{rms}}$ ($\sim$31%), which agrees well with the finding by Moser et al. [12] that w_{rms} shows a larger variation than u_{rms} as Re_τ increases. Especially, the value of $\tau_{1_{rms}}$ seems to be nearly saturated at around $0.4\tau_w$ at Re_τ=640. This can also be observed from the literature. That is, Alfredsson et al. [36] carried out an experiment using a hot-film probe and specially designed sensors for the channel and boundary layer flows and reported that $\tau_{1_{rms}}=0.40\tau_w$. Recently, Fischer et al. [35] conducted an experiment using a laser Doppler anemometry and reported that the limiting value of $\tau_{1_{rms}}$ tends to approach $0.40\tau_w$ at relatively high Reynolds number. More recently, Metzger and Klewicki [10] performed an experiment using a hot-wire probe in a turbulent boundary layer at high Reynolds numbers and indicated that the wall value of the spanwise vorticity fluctuations, i.e., $\tau_{1_{rms}}$, does
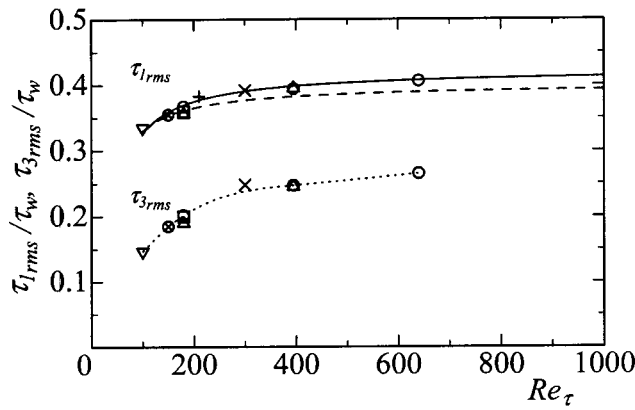
Fig. 9 Variations of the rms wall shear-stress fluctuations as a function of the Reynolds number. (○) present study; (▽), Kuroda et al. [31]; (+), Gilbert and Kleiser [32]; (⊗), Kuroda et al. [33]; (△), Antonia and Kim [11]; (×), Günther et al. [34]; (□), Jeon et al. [3]; (——), fitting for $\tau_{1_{rms}}/\tau_w$ by Fischer et al. [35] from DNS; (— — —), fitting for $\tau_{1_{rms}}/\tau_w$ by Fischer et al. [35] from experiments; (- - -), fitting for $\tau_{3_{rms}}/\tau_w$.

Fig. 10 One-dimensional wave number power spectra of τ_1 and τ_3 normalized by the mean-square values: (a) streamwise wave number; (b) spanwise wave number. (○), Wietrzak and Lueptow [37] ($Re_\tau = 896$); (△), Nepomuceno and Lueptow [38] ($Re_\tau = 751$).

not vary with the Reynolds number when the Reynolds number is sufficiently high, although they showed a logarithmic increase in the peak value of u'. Also, recent DNSs of turbulent channel flow indicated that $\tau_{1_{rms}} = 0.405 \tau_w$ at $Re_\tau = 590$ [12] and $0.409 \tau_w$ at $Re_\tau = 640$ [13]. From the past and present results, therefore, it may be concluded that $\tau_{1_{rms}}$ is about $0.4 \tau_w$ at sufficiently high Reynolds numbers.

Conducting another investigation on the Reynolds-number dependence of the wall shear-stress fluctuations as the mean-square values, i.e., $\tau_{1_{rms}}^2$ and $\tau_{3_{rms}}^2$, the increase in $\tau_{1_{rms}}^2$ and $\tau_{3_{rms}}^2$ from $Re_\tau = 180$ to 640 is 0.030 and 0.029, respectively. Interestingly, almost the same increase is obtained in the streamwise and spanwise directions.

4.1.1 Power Spectra. The power spectra of τ_1 and τ_3 are defined as

$$\int_0^\infty \phi(k_x) dk_x = \int_0^\infty \phi(k_z) dk_z = \tau_{1_{rms}}^2 \quad \text{or} \quad \tau_{3_{rms}}^2, \qquad (4)$$

where $\phi(k_x)$ and $\phi(k_z)$ are the power spectra. As was shown in Fig. 9, the mean-square values, i.e., integrations of the spectra over the wave number, increase with increasing Reynolds number. Accordingly, the streamwise- and spanwise-wave number spectra of τ_1 and τ_3 are normalized by their own mean-square values and are shown in Fig. 10. The frequency spectra measured by Wietrzak and Lueptow [37] ($Re_\tau = 896$) and Nepomuceno and Lueptow [38] ($Re_\tau = 751$) are also plotted for comparison, using Taylor's hypothesis with a convection velocity of $0.53 U_o$ [3], where U_o is the freestream velocity or channel centerline velocity. Agreement between the present result and the measurement results [37,38] is satisfactory, although there exists a discernible difference at high wave numbers. This difference may be caused by the fact that the convection velocity associated with the energy containing eddy (i.e., low wave number) is used for all wavenumbers.

In Fig. 10(a), the streamwise wave number power spectra of τ_1 and τ_3 show good collapse at the whole range of wave numbers for the three Reynolds numbers, meaning that the contributions from small, intermediate, and large scales in the streamwise direction to the rms values are essentially the same, at least for the Reynolds number range investigated. In contrast, the spanwise wave number power spectra of τ_1 and τ_3 show collapse at small scales (i.e., at large wave numbers) only, whereas they exhibit an
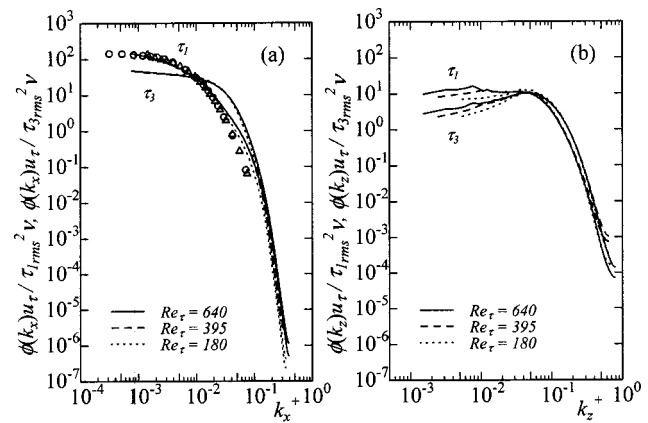
increase in power at large scales (i.e., at small wave numbers) with increasing Reynolds number [Fig. 10(b)]. This indicates that the contribution from large scales in the spanwise direction to the rms values increases with increasing Reynolds number. Moreover, it is interesting to note that local peaks are observed at low wave numbers for $Re_\tau = 395$ and 640 and the corresponding wave numbers in walls units become smaller with increasing Reynolds number, indicating that very large-scale structures should exist in τ_1 and τ_3 for high Reynolds numbers.

In order to examine the behavior of these local peaks, the spanwise spectra of τ_1 and τ_3 normalized with τ_w and δ are redrawn for all three Reynolds numbers at $k_z \delta < 100$ in linear scales and are shown in Fig. 11. In this figure, there appears a clear local peak at $k_z \delta \approx 5$ in the spectra of τ_1 at $Re_\tau = 395$ and 640, where the wavelength corresponding to this wave number is 1.3δ. Moreover, this local peak is identical with that of the near-wall spanwise premultiplied spectra of u', which is closely associated with the most energetic peak in the outer layer [see Figs. 6(b) and 6(c)]. These results indicate that the VLSMs in the outer layer maintain a certain influence even upon the wall flow variables such as the wall shear stresses at high Reynolds number cases. Moreover, it can be seen in Fig. 11 that the local peak in the spanwise spectra of τ_1 becomes more prominent with increasing Reynolds number. At $Re_\tau = 640$, an excess of the power at the local peak over the averaged power in the nearly constant range, $k_z \delta = 10-30$, is about 3% of the total power. In contrast, integrating the spectra over the range of wave numbers, $k_z \delta = 0-10$, in which the spectra
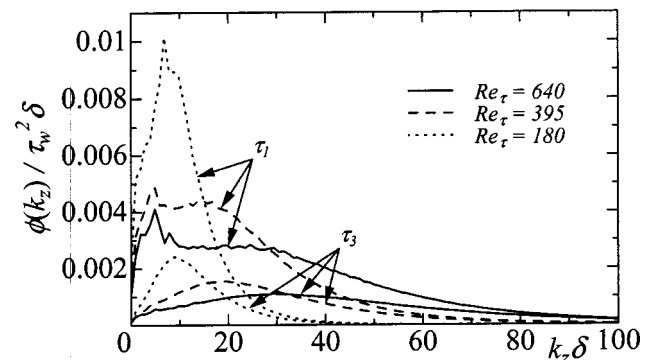
Fig. 11 One-dimensional spanwise wave number power spectra of τ_1 and τ_3 normalized by τ_w and δ in linear scales
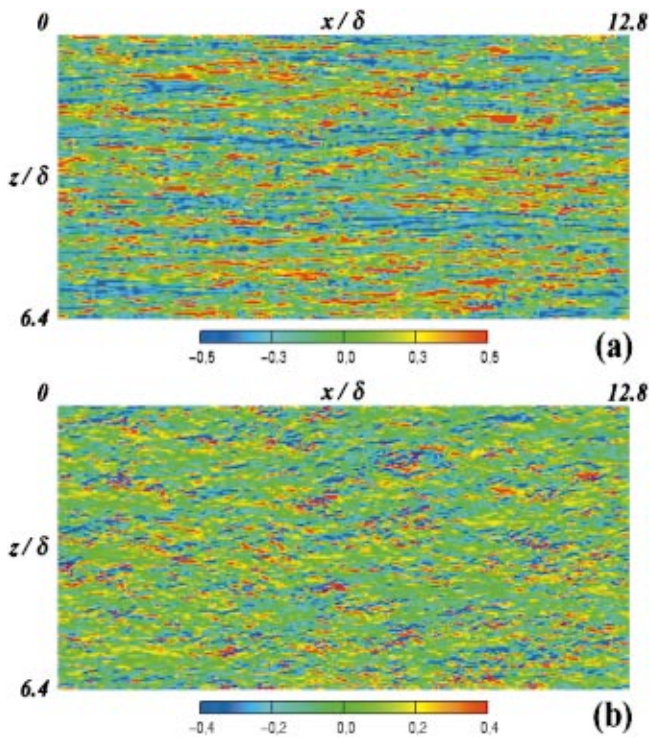
Fig. 12 Contours of the instantaneous wall shear-stress fluctuations for $Re_\tau=640$; (a) τ_1; (b) τ_3

Fig. 13 Enlarged view of Fig. 12: (a) τ_1; (b) τ_3

show the local peak, the power contained in the range of the wave numbers is about 20% of the total power, suggesting that the importance of the low wave numbers in the spanwise direction increases with increasing Reynolds number. At the low Reynolds number of $Re_\tau=180$, we see local peaks at $k_z\delta\simeq7$ and 9, which correspond to $\lambda_z/\delta\simeq0.9$ and 0.7, respectively. The latter wavelength is very close to the streak spacing at this Reynolds number. It is not so clear why we have the first peak at $k_z\delta\simeq7$ rather than at $k_z\delta\simeq5$ for $Re_\tau=180$. We consider the first peak at $k_z\delta\simeq7$ to be the result of a low Reynolds-number effect because the separation of two scales (streaky structure near the wall and very large-scale structure in the outer layer) is not so evident at $Re_\tau=180$ as shown in Fig. 6(a). On the other hand, a clear local peak is not observed at $k_z\delta\simeq5$ either in the spectra of τ_3 in Fig. 11, because the power at this spanwise wave number is much smaller than the maximum power at $k_z^+=0.06$ corresponding to the streak spacing unlike the case of τ_1 at high Reynolds number [see Fig. 10(b)].

One may wonder if these local peaks in Figs. 10 and 11 come from insufficient time averaging, and they could be due to the statistical noise. In order to investigate this issue, we performed a long time integration for the case of $Re_\tau=395$, where the sampling period is $50L_x/u_m$. Indeed, with longer time averaging, the spectra become smoother but the large local peak still exists.

4.1.2 Instantaneous Flow Fields. In this section, we show from instantaneous flow fields that there exist very large-scale patterns in the wall shear-stress fluctuations and the corresponding length scales are closely associated with the peaks at low wave numbers in the spanwise spectra in Fig. 10(b).

Figure 12 shows the contours of the instantaneous wall shear-stress fluctuations for $Re_\tau=640$ in the full computational domain. In the case of τ_1, a few (or several) streaks of negative τ_1's (blue color) are packed together and make a group in space (called a "negative dominant" region, hereafter). Moreover, this dense clustering of negative τ_1's clearly exhibits a very large-scale pattern.

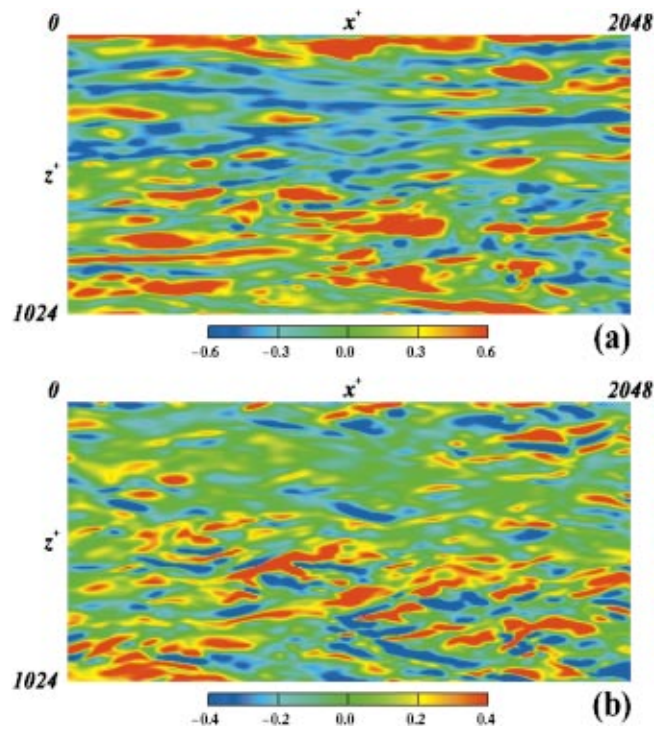In the case of τ_3 [Fig. 12(b)], there exist two substantially dif-

ferent regions: one of them consists of dense clustering of strong positive and negative τ_3's (called an "active" region, hereafter) and the other is a region of weak τ_3's (called an "inactive" region, hereafter). A careful inspection of the instantaneous flow fields indicates that the active region of τ_3 is closely associated with the group of positive τ_1's and the inactive one occurs where the group of negative τ_1's exists (see Fig. 13 for the enlarged view).

To inspect the very large-scale pattern of τ_1 in more detail, a filtering procedure is applied to the instantaneous field shown in Fig. 12(a). A top-hat filter defined as

$$\tilde{\tau}_1(x,z)=\frac{1}{4\ell_x\ell_z}\int_{-\ell_x}^{\ell_x}\int_{-\ell_z}^{\ell_z}\tau_1(x+\xi,z+\zeta)d\zeta d\xi \qquad (5)$$

is employed, where a tilde denotes a filtered value. Referring to Komminaho et al. [40], the streamwise filter length ℓ_x is chosen as the integral scale and the spanwise filter length ℓ_z is roughly the same length as the first zero-crossing point of the spanwise two-point correlation. The filtered instantaneous field with $\ell_x^+=232$ and $\ell_z^+=44$ is shown in Fig. 14(a), where very large-scale patterns with a spanwise spacing of about $1.3-1.6\delta$ (about 1000 in wall units for $Re_\tau=640$) are more clearly illustrated. This spanwise spacing corresponds to the spanwise wave number of $k_z\delta=4-5$ (or $k_z^+=0.006-0.008$) at which the spectrum of τ_1 shows a local peak at $Re_\tau=640$ (see Fig. 11). In order to examine the interaction between the inner and outer layers, the top view of the instantaneous low-speed regions in the outer layer ($u'/u'_{rms}<-1.75$) shown in Fig. 8(b) is superimposed on the filtered τ_1 shown in Fig. 14(a). The resultant figure is given in Fig. 14(b). It is clear from this figure that the negative dominant regions of τ_1 are mostly overshadowed by the low-speed regions in the VLSMs.

To examine this point more quantitatively, we introduce a function called an overlap ratio (OLR). In the OLR, variables ϕ and ψ are binarized to be either 0 or 1 based on a certain threshold, and the binarized ones are represented by $\hat{\phi}$ and $\hat{\psi}$. Then, the OLR is defined as the ratio of the overlapping area between $\hat{\phi}$ and $\hat{\psi}$ to the area of either $\hat{\phi}$ or $\hat{\psi}$:
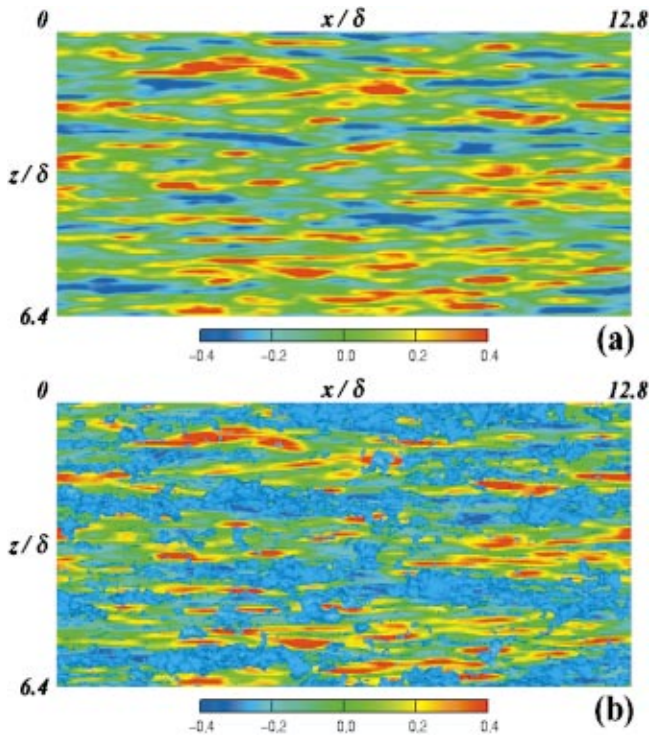
Fig. 14 Contours of the filtered τ_1 and top view of the low-speed regions in the VLSMs for Re_τ=640: (a) filtered τ_1; (b) top view of the low-speed regions in the outer layer (u'/u'_{rms} <−1.75 denoted as blue iso-surfaces) shown in Fig. 8(b), which is superimposed on the filtered τ_1 shown in Fig. 14(a)
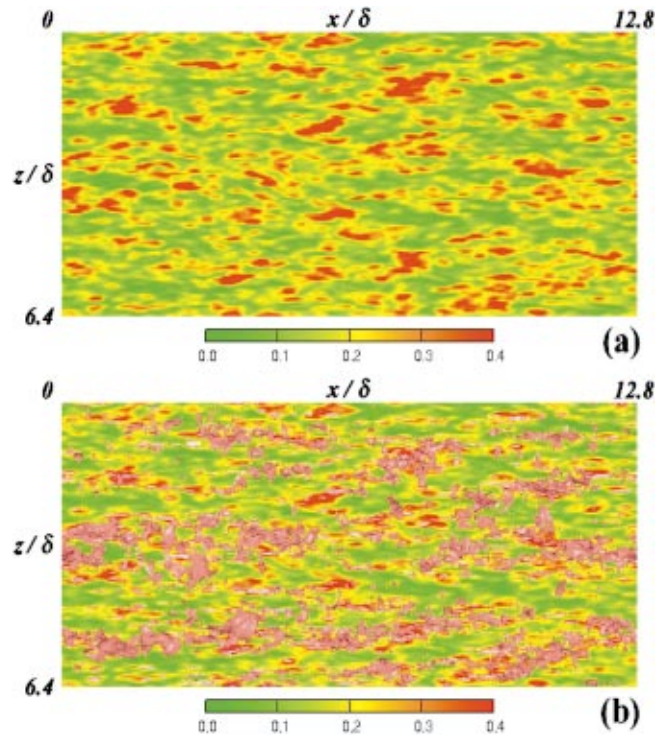
Fig. 15 Contours of the filtered τ_3 and top view of the high-speed regions in the VLSMs for Re_τ=640: (a) filtered τ_3; (b) top view of the high-speed regions in the outer layer (u'/u'_{rms} >1.75 denoted as red iso-surfaces) shown in Fig. 8(b), which is superimposed on the filtered τ_3 shown in Fig. 15(a)

$$\text{OLR}(\phi<\phi_0 \text{ or } \phi>\phi_0|\psi<\psi_0 \text{ or } \psi>\psi_0)=\sum \hat{\phi}\hat{\psi}/\sum \hat{\psi}^2, \quad (6)$$

where ϕ_0 and ψ_0 are the threshold values. We obtain the OLR between the filtered τ_1 (i.e., $\tilde{\tau}_1$) and the projected area of high- or low-speed regions in the VLSMs. First, $\tilde{\tau}_1$ is binarized with a threshold of $\tilde{\tau}_{1_0}/\tilde{\tau}_{1_{rms}}=\pm 1.5$. Next, the projected and binarized high- and low-speed regions are obtained through the following operations: (i) u' is binarized with respect to $u'_0/u'_{rms}=\pm 1.75$, (ii) the binarized values $\hat{u}'$ are integrated along the wall-normal direction up to the channel center, and (iii) the integrated values are rebinarized to be either 0 or 1 with a threshold of 1. This procedure reveals that the OLR between the low-speed region in the VLSMs and the negative region of τ_1 is $\text{OLR}(u'<-1.75u'_{rms}|\tilde{\tau}_1<-1.5\tilde{\tau}_{1_{rms}})=0.76$, whereas the OLR between the low-speed region in VLSMs and the positive region of τ_1 is $\text{OLR}(u'<-1.75u'_{rms}|\tilde{\tau}_1>1.5\tilde{\tau}_{1_{rms}})=0.20$. Moreover, it is found that the OLR between the high-speed region in the VLSMs and the positive region of τ_1 is $\text{OLR}(u'>1.75u'_{rms}|\tilde{\tau}_1>1.5\tilde{\tau}_{1_{rms}})=0.65$, whereas the OLR between the high-speed region in VLSMs and the negative region of τ_1 is $\text{OLR}(u'>1.75u'_{rms}|\tilde{\tau}_1<-1.5\tilde{\tau}_{1_{rms}})=0.19$. These results clearly indicate that the very large-scale structure observed in τ_1 is essentially associated with the VLSMs existing in the outer layer of the flow.

Now we will examine the active and inactive regions of τ_3 in detail. To emphasize the difference between these two regions, the filtering procedure is again applied to τ_3. In the filtering of τ_3, its absolute value is filtered to avoid possible cancellation of τ_3 because its positive and negative values lie quite close to each other. The filtered instantaneous field with $\ell_x^+=80$ and $\ell_z^+=28$ is shown in Fig. 15(a), where the active (red color) and inactive (green

color) regions are more clearly seen for τ_3. From Figs. 14(a) and 15(a), one can easily notice that the active region of τ_3 corresponds much more often to the positive dominant region of τ_1 than the negative one of τ_1. The OLR between the positive region of τ_1 and the active region of τ_3 is $\text{OLR}(\tilde{\tau}_1>1.0\tilde{\tau}_{1_{rms}}||\tilde{\tau}_3|>1.5\tilde{\tau}_{3_{rms}})=0.43$, whereas the OLR between the negative region of τ_1 and the active region of τ_3 is $\text{OLR}(\tilde{\tau}_1<-1.0\tilde{\tau}_{1_{rms}}||\tilde{\tau}_3|>1.5\tilde{\tau}_{3_{rms}})=0.02$, which clearly supports the visual impression mentioned above.

To examine the relation between τ_3 and the VLSMs, the top view of the high-speed regions in the outer layer (u'/u'_{rms} >1.75) shown in Fig. 8(b) is superimposed on the filtered τ_3 shown in Fig. 15(a), and the result is given in Fig. 15(b). The OLR between the high-speed region in the VLSMs and the active region of τ_3 is $\text{OLR}(u'>1.75u'_{rms}||\tilde{\tau}_3|>1.5\tilde{\tau}_{3_{rms}})=0.55$, whereas the OLR between the high-speed region in VLSMs and the inactive region of τ_3 is $\text{OLR}(u'>1.75u'_{rms}||\tilde{\tau}_3|<0.3\tilde{\tau}_{3_{rms}})=0.16$. Thus, the active region of τ_3 mostly corresponds to the high-speed region in the VLSMs.

5 Summary and Conclusions

In this study, we obtained the mean flow variables, root-mean-square (rms) values, power spectra, and two-point correlations from direct numerical simulation of turbulent channel flow at Re_τ=180, 395, and 640, and examined the very large-scale structures and their effects on the wall shear-stress fluctuations.

It was shown that very large-scale structures with a spanwise spacing of $1.3-1.6\delta$ exist in the outer layer and that they certainly contribute to the inner layer structures for high Reynolds number. Moreover, it was found that the effects of the very large-scale structures in the outer layer on the mean flow variables and the turbulence quantities are negligibly small for the Reynolds num-

ber range investigated, whereas those of the very large-scale structures on the spanwise premultiplied spectra at long wavelengths are significant.

The effects of the very large-scale structures were also found even in the wall shear-stress fluctuations. That is, the local peaks appeared in the spanwise wave number power spectra of τ_1 and τ_3 at low wave numbers for $\mathrm{Re}_\tau = 395$ and 640 and they became more prominent with increasing Reynolds number, indicating that very large-scale structures exist even in τ_1 and τ_3 for high Reynolds number.

The instantaneous flow field showed that the very large-scale structures appear not only in the outer layer but also at the wall for high Reynolds number. That is, the very large-scale motions with a streamwise extent of more than 3δ and a spanwise spacing of $1.3-1.6\delta$ existed in the outer layer, and very large-scale structures with dense clustering flow patterns appeared in the wall shear-stress fluctuations. The filtering procedure disclosed the very large-scale structures in τ_1 and τ_3 more clearly. Notably, it was indeed found in τ_1 that the very large-scale structures with a spanwise spacing of about $1.3-1.6\delta$ exist. This spanwise spacing corresponds to the spanwise wave number of $k_z\delta = 4-5$ at which the spectrum of τ_1 shows a local peak at $\mathrm{Re}_\tau = 395$ and 640.

Inspection of the interaction between the inner and outer layers revealed that the positive and negative dominant regions in τ_1 correspond, respectively, to the high- and low-speed regions in the very large-scale motions in the outer layer, whereas the active region in τ_3 corresponds to the high-speed region in the very large-scale motions. These results indicate that the very large-scale structures existing in τ_1 and τ_3 for $\mathrm{Re}_\tau = 640$ are essentially phenomena associated with the very large-scale motions existing in the outer layer of the flow.

The database is posted at http://murasun.me.noda.tus.ac.jp.

Acknowledgments

References

[1] Choi, H., and Moin, P., 1990, "On the Space-Time Characteristics of Wall Pressure Fluctuations," Phys. Fluids A, **2**, pp. 1450–1460.

[2] Farabee, T. M., and Casarella, M. J., 1991, "Spectral Features of Wall Pressure Fluctuations Beneath Turbulent Boundary Layers," Phys. Fluids A, **3**, pp. 2410–2420.

[3] Jeon, S., Choi, H., Yoo, J. Y., and Moin, P., 1999, "Space-Time Characteristics of the Wall Shear-Stress Fluctuations in a Low-Reynolds-Number Channel Flow," Phys. Fluids, **11**, pp. 3084–3094.

[4] Kim, J., 1989, "On the Structure of Pressure Fluctuations in Simulated Turbulent Channel Flow," J. Fluid Mech., **205**, pp. 421–451.

[5] Bullock, K. J., Cooper, R. E., and Abernathy, F. H., 1978, "Structural Similarity in Radial Correlations and Spectra of Longitudinal Velocity Fluctuations in Pipe Flow," J. Fluid Mech., **88**, pp. 585–608.

[6] Naguib, A. M., and Wark, C. E., 1992, "An Investigation of Wall-Layer Dynamics Using a Combined Temporal Filtering and Correlation Technique," J. Fluid Mech., **243**, pp. 541–560.

[7] Hites, M. H., 1997, "Scaling of High-Reynolds Number Turbulent Boundary Layers in the National Diagnostic Facility," Ph.D. thesis, Illinois Institute of Technology.

[8] Kim, K. C., and Adrian, R. J., 1999, "Very Large-Scale Motion in the Outer Layer," Phys. Fluids, **11**, pp. 417–422.

[9] Österlund, J. M., 1999, "Experimental Studies of Zero Pressure-Gradient Turbulent Boundary Layer Flow," Ph.D. thesis, Department of Mechanics, Royal Institute of Technology, Stockholm.

[10] Metzger, M. M., and Klewicki, J. C., 2001, "A Comparative Study of Near-Wall Turbulence in High and Low Reynolds Number Boundary Layers," Phys. Fluids, **13**, pp. 692–701.

[11] Antonia, R. A., and Kim, J., 1994, "Low-Reynolds-Number Effects on Near-Wall Turbulence," J. Fluid Mech., **276**, pp. 61–80.

[12] Moser, R. D., Kim, J., and Mansour, N. N., 1999, "Direct Numerical Simulation of Turbulent Channel Flow up to $\mathrm{Re}_\tau = 590$," Phys. Fluids, **11**, pp. 943–945.

[13] Abe, H., Kawamura, H., and Matsuo, Y., 2001, "Direct Numerical Simulation of a Fully Developed Turbulent Channel Flow With Respect to the Reynolds Number Dependence," ASME J. Fluids Eng., **123**, pp. 382–393.

[14] del Álamo, J. C., and Jiménez, J., 2001, "Direct Numerical Simulation of the Very Anisotropic Scales in a Turbulent Channel," Center for Turbulence Research Annual Research Briefs, pp. 329–341.

[15] del Álamo, J. C., and Jiménez, J., 2003, "Spectra of the Very Large Anisotropic Scales in Turbulent Channels," Phys. Fluids, **15**, pp. L41–L44.

[16] Abe, H., and Kawamura, H., 2002, "A Study of Turbulence Thermal Structure in a Channel Flow Through DNS up to $\mathrm{Re}_\tau = 640$ With $\mathrm{Pr} = 0.025$ and 0.71," Proceedings of 9th European Turbulence Conference, pp. 399–402.

[17] Jiménez, J., Flores, O., and García-Villalba, M., 2001, "The Large-Scale Organization of Autonomous Turbulent Wall Regions," Center for Turbulence Research Annual Research Briefs, pp. 317–327.

[18] Dukowics, J. K., and Dvinsky, A. S., 1992, "Approximate Factorization as a High Order Splitting for the Implicit Incompressible Flow Equations," J. Comp. Physiol., **102**, pp. 336–347.

[19] Morinishi, Y., Lund, T. S., Vasilyev, O. V., and Moin, P., 1998, "Fully Conservative Higher Order Finite Difference Schemes for Incompressible Flow," J. Comp. Physiol., **143**, pp. 90–124.

[20] Jiménez, J., 1998, "The Largest Scales of Turbulent Wall Flows," Center for Turbulence Research Annual Research Briefs, pp. 137–154.

[21] Kawamura, H., Abe, H., and Shingai, K., 2000, "DNS of Turbulence and Heat Transport in a Channel Flow With Different Reynolds and Prandtl Numbers and Boundary Conditions," Proceedings of 3rd International Symposium Turbulence, Heat and Mass Transfer, pp. 15–32.

[22] Hussain, A. K. M. F., and Reynolds, W. C., 1975, "Measurements in Fully Developed Turbulent Channel Flow," J. Fluids Eng., **97**, pp. 568–580.

[23] Spalart, P. R., 1988, "Direct Simulation of a Turbulent Boundary Layer up to $R_\theta = 1410$," J. Fluid Mech., **187**, pp. 61–98.

[24] Falco, R. E., 1977, "Coherent Motions in the Outer Region of Turbulent Boundary Layers," Phys. Fluids, **20**, pp. S124–SS132.

[25] Brown, G. L., and Thomas, A. S. W., 1977, "Large Structure in a Turbulent Boundary Layer," Phys. Fluids, **20**, pp. S243–S252.

[26] Adrian, R. J., Meinhart, C. D., and Tomkins, C. D., 2000, "Vortex Organization in the Outer Layer Region of the Turbulent Boundary Layer," J. Fluid Mech., **422**, pp. 1–54.

[27] Liu, Z., Adrian, R. J., and Hanratty, T. J., 2001, "Large-Scale Modes of Turbulent Channel Flow: Transport and Structure," J. Fluid Mech., **448**, pp. 53–80.

[28] Smith, C. R., and Metzler, S. P., 1983, "The Characteristics of Low-Speed Streaks in the Near-Wall Region of a Turbulent Boundary Layer," J. Fluid Mech., **129**, pp. 27–54.

[29] Nakagawa, H., and Nezu, I., 1981, "Structure of Space-Time Correlations of Bursting Phenomena in an Open-Channel Flow," J. Fluid Mech., **104**, pp. 1–43.

[30] Perry, A. E., Henbest, S., and Chong, M. S., 1986, "A Theoretical and Experimental Study of Wall Turbulence," J. Fluid Mech., **165**, pp. 163–199.

[31] Kuroda, A., Kasagi, N., and Hirata, M., 1989, "A Direct Numerical Simulation of the Fully Developed Turbulent Channel Flow at a Very Low Reynolds Number," Proceedings of the International Symposium on Computational Fluid Dynamics, Nagoya, pp. 1174–1179.

[32] Gilbert, N., and Kleiser, L., 1991, "Turbulence Model Testing With the Aid of Direct Numerical Simulation Results," Proceedings of the Eighth Symposium on Turbulent Shear Flows, TU of München, pp. 26.1.1–26.1.6.

[33] Kuroda, A., Kasagi, N., and Hirata, M., 1993, "Direct Numerical Simulation of the Turbulent Plane Couette-Poiseuille Flows: Effect of Mean Shear on the Near Wall Turbulence Structures," Proceedings of the Ninth Symposium on Turbulent Shear Flows, Kyoto, pp. 8.4.1–8.4.6.

[34] Günther, A., Papavassiliou, D. V., Warholic, M. D., and Hanratty, T. J., 1998, "Turbulent Flow in a Channel at a Low Reynolds Number," Exp. Fluids, **25**, pp. 503–511.

[35] Fischer, M., Jovanović, J., and Durst, F., 2001, "Reynolds Number Effects in the Near-Wall Region of Turbulent Channel Flows," Phys. Fluids, **13**, pp. 1755–1767.

[36] Alfredsson, P. H., Johansson, A. V., Haritonidis, J. H., and Eckelmann, H., 1988, "The Fluctuating Wall-Shear Stress and the Velocity Field in the Viscous Sublayer," Phys. Fluids, **31**, pp. 1026–1033.

[37] Wietrzak, A., and Lueptow, R. M., 1994, "Wall Shear Stress and Velocity in a Turbulent Axisymmetric Boundary Layer," J. Fluid Mech., **259**, pp. 191–218.

[38] Nepomuceno, H. G., and Lueptow, R. M., 1997, "Pressure and Shear Stress Measurements at the Wall in a Turbulent Boundary Layer on a Cylinder," Phys. Fluids, **9**, pp. 2732–2739.

[39] Robinson, S. K., 1991, "The Kinematics of Turbulent Boundary Layer Structure," NASA TM, 103859.

[40] Komminaho, J., Lundbladh, A., and Johansson, A. V., 1996, "Very Large Structures in Plane Turbulent Couette Flow," J. Fluid Mech., **320**, pp. 259–285.